Journal of Alloys and Compounds 506 (2010) 412–417

Contents lists available at ScienceDirect

Journal of Alloys and Compounds

journal homepage: www.elsevier.com/locate/jallcom

First-principles study of elastic and electronic properties of $MgZn_2$ and $ScZn_2$ phases in Mg–Sc–Zn alloy

Meng-Meng Wu[a], Li Wen[a], Bi-Yu Tang[a,b,*], Li-Ming Peng[c], Wen-Jiang Ding[c]

[a] School of Chemistry and Chemical Engineering, Guangxi University, Nanning 530004, China
[b] Key Laboratory of Low Dimensional Materials & Application Technology, Ministry of Education, Department of Physics, Xiangtan University, Hunan Province 411105, China
[c] Light Alloy Net Forming National Engineering Research Center, School of Materials Science and Engineering, Shanghai Jiaotong University, Shanghai 200030, China

ARTICLE INFO

Article history:
Received 1 April 2010
Received in revised form 30 June 2010
Accepted 6 July 2010
Available online 14 July 2010

Keywords:
First-principles calculations
Elastic constants
Mechanical properties
Electronic structure
Mg–Sc–Zn alloy

ABSTRACT

The structural, electronic and elastic properties of typical hexagonal-close-packed $MgZn_2$ and $ScZn_2$ phases in Mg–Sc–Zn alloy were investigated by means of first-principles calculations within the framework of density functional theory (DFT). The calculated lattice constants were in good agreement with the experimental values. The obtained cohesive energy and formation enthalpy of both phases are negative, showing their structural stability from energetic point of view. The five independent elastic constants were calculated, and then the bulk modulus B, shear modulus G, Young's modulus E and Poisson's ratio ν of polycrystalline aggregates were derived. The ductility and plasticity of the $MgZn_2$ and $ScZn_2$ phases were further discussed. The elastic anisotropy of the two phases was also analyzed. Finally, the electronic density of states (DOS) and charge density distribution were also calculated to reveal the underlying mechanism of structural stability and mechanical properties.

1. Introduction

In recent years, magnesium alloys have been receiving a great deal of attention in the fields of microelectronics, automobile and aerospace industries [1–3] because of their low density, high specific strength and good stiffness [4]. However, the application of magnesium alloys in modern industry is still limited due to the restrained mechanical properties [5], especially the poor creep, corrosion and ignition resistance at high temperature [6]. Therefore, much work has been focused on improving the properties of the alloys. It has been found that alloying by addition of rare earth elements is an effective method to improve the microstructure and mechanical properties of magnesium alloys [6,7]. Furthermore, many experimental results revealed that the addition of Zn and Sc plays a very important role in optimizing the microstructure and mechanical properties of magnesium alloys [8,9]. Up to now, several alloy systems have been studied such as the Mg–Zn and Mg–RE binary systems on one hand, and ternary Mg–Zn–RE system on the other hand.

All of these alloy systems exhibit age-hardening response, especially the Mg–Zn system alloys belong to the stronger precipitation-hardenable Mg alloys. As the equilibrium solid solubility of zinc in magnesium decreases substantially with temperature decreasing, a controlled decomposition of the supersaturated solid solution of zinc in magnesium can produce a remarkable age-hardening effect [10,11]. Based on the binary Mg–Zn phase diagram [12], there are five intermetallic phases in the Mg–Zn system, namely Mg_7Zn_3, MgZn, Mg_2Zn_3, $MgZn_2$ and Mg_2Zn_{11}, of which $MgZn_2$ is the most important strengthening phase [13,14]. Therefore, the study on $MgZn_2$ phase is of great importance and has led to a renewed interest in the research and development of Mg-based alloys. Sc is another important alloying rare earth element in magnesium alloys, and the addition of Sc to Mg–Zn-based alloys has been found to be effective in improving the mechanical properties of the alloy at both room and high temperature [15]. $ScZn_2$ is a typical and important phase in Mg–Zn-based alloys. When Zn and Sc are added to Mg simultaneously, long period stacking ordered (LPSO) phases are very likely to come out instead of ordered intermetallic precipitates. Especially when Zn is added in dilute quantity, which is done in practice, the formation of LPSO phases is frequently observed in typical $Mg_{97}Y_2Zn_1$ alloy under rapid solidification processing [16,17]. However, when Zn content is relatively high, $ScZn_2$ and $MgZn_2$ phases in Mg-based alloy are also always formed by traditional method. The strengthening phase $MgZn_2$ could be formed in the temperature range of 346–316 °C during solidification of the Mg–8Zn–1.5MM (misch metal) alloy [11], and the strengthening phase $ScZn_2$ is also obtained in the temperature range of

* Corresponding author at: School of Chemistry and Chemical Engineering, Guangxi University, Nanning 530004, China. Tel.: +86 731 58292195; fax: +86 731 58292468.
E-mail addresses: tangbiyu@gxu.edu.cn, tangbiyu@xtu.edu.cn (B.-Y. Tang).

0925-8388/$ – see front matter © 2010 Elsevier B.V. All rights reserved.
doi:10.1016/j.jallcom.2010.07.018

1900–25 °C during solidification of the Sc–Zn system [18]. The competition between precipitates and LPSO phases is a complicate process, which needs a further investigation. To achieve this goal, the structural stability and elastic properties of ordered intermetallic precipitates have been studied firstly here. Many experiments have been carried out to investigate the $ScZn_2$ and $MgZn_2$ phases in Mg-based alloys [13,18], and theoretical studies on the structure and vibrational properties of $MgZn_2$ precipitate by means of first-principles are also reported [19], especially Datta et al. [20] have investigated the structural feature as well as SFES in Mg with 2 at.% Zn, and their study throws considerable light on plastic properties of LPSO phase. However, the theoretical investigations on the elastic properties of $MgZn_2$ and $ScZn_2$ are scarce.

In the present work, the first-principles calculations are carried out to investigate the structural, elastic and electronic properties of the binary phases $MgZn_2$ and $ScZn_2$ with C14 structure in Mg-based alloys. The results are discussed in comparison with the available experimental values, which would be useful for the optimization and design of the relevant alloys.

2. Computational method

The present calculations are carried out using density functional theory (DFT) [21] as implemented in the Vienna Ab Initio Simulation Package (VASP) code [22]. It is well known that density functional theory (DFT) with the standard local density approximation (LDA) does not accurately describe the properties of 3d transition metals, and the errors can largely be removed by generalized gradient approximation (GGA) [23]. So the Perdew–Wang (PW91) version of the generalized gradient approximation (GGA) [24] is used to describe the exchange-correlation energy functional and the projector augmented wave (PAW) method [25] has been used in the present work. The electron configuration for Mg treats 3s states as valence state, and others are described by 3d, 4s valence states for Zn, 3p, 4s, 3d valence states for Sc, respectively. Two parameters that affect the accuracy of calculation are the kinetic energy cut-off which determines the number of plane waves in the expansion and the number of special *k*-points used for the Brillouin zone (BZ) integration. The cut-off energy of plane wave is set at 350 eV for $MgZn_2$ and $ScZn_2$. The Brillouin zone integration uses Gamma centered Monkhors-Pack grids [26] of $8 \times 8 \times 6$ mesh for optimizing geometry and calculating elastic constants, and $12 \times 12 \times 8$ for calculation of the density of states (DOS). The geometry optimization is performed by full relaxation until the total energy changes within 10^{-4} eV/atom and the Hellmann–Feynman force on all atoms is less than 10^{-2} eV/Å. The density of states (DOS) and total energy calculations are performed using the linear tetrahedron method with Blöchl correction [27].

3. Results and discussion

3.1. Crystal structure and stability

Binary precipitates $MgZn_2$ and $ScZn_2$ belong to the hexagonal structure with the space group $P6_3/mmc$ (*#194*) and contain

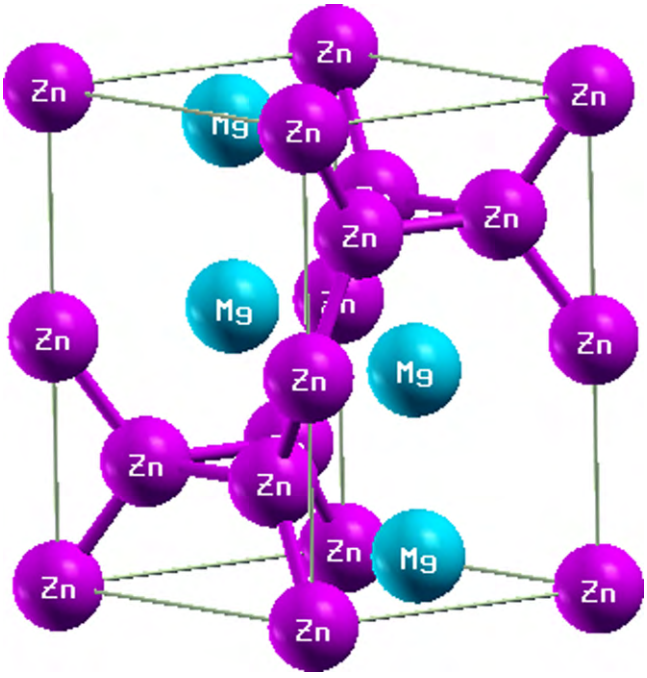

Fig. 1. Crystal cell for $Mg(Sc)Zn_2$. The red spheres are Zn atoms and the blue spheres are Mg(Sc) atoms. (For interpretation of the references to color in this figure legend, the reader is referred to the web version of the article.)

12 atoms per unit cell [18,28]. In unit cell of both phases, Mg(Sc) atoms are located on 4f sites and Zn atoms on 2a and 6h sites, as shown in Fig. 1. After structural optimization, the obtained internal coordinates of atoms for both $MgZn_2$ and $ScZn_2$ are 4f (0.333, 0.667, 0.063), 2a (0, 0, 0) and 6h (0.833, 0.667, 0.250), which are in accordance with the experimental results [18,28]. The equilibrium volume V_0 and bulk modulus B_0 of $MgZn_2$ and $ScZn_2$ are determined by fitting the calculated total energy at different volumes to a Birch–Murnaghan equation of state (EOS) [29]. The obtained results are listed in Table 1, together with available experimental values. It can be seen that the obtained lattice parameters are consistent with the available experimental values [18,28], the fairly good agreement between theoretical and experimental results shows that the present calculation is highly reliable.

The structural stability of $Mg(Sc)Zn_2$ is investigated by means of cohesive energy E_{coh} which is defined as the energy that is needed when the crystal decomposes into a single atom. The lower the cohesive energy is, the more stable the crystal structure is [30]. The cohesive energy E_{coh} of $MgZn_2$ and $ScZn_2$ crystal cells were calculated by

$$E_{coh} = \frac{E_{tot} - N_A E^A_{\text{atom}} - N_B E^B_{\text{atom}}}{N_A + N_B} \quad (1)$$

where E_{tot} is the total energy of the unit cell, E^A_{atom} and E^B_{atom} are the total energies of the isolated *A* and *B* atoms in the free state. They are calculated by means of a large box within which the correspond-

Table 1
The calculated and experimental lattice constants (*a* and *c*, in Å), volumes of unit cell V_0 (in Å^3/cell), bulk modulus B_0 (in GPa), as well as the cohesive energy E_{coh} (eV/atom) and formation enthalpy ΔH (eV/atom) for $MgZn_2$, $ScZn_2$ binary phases.

Material	Lattice constants (Å)		V_0	B_0	E_{coh}	ΔH
	Cal.	Exp.				
$MgZn_2$	$a = 5.2040$, $c = 8.5398$	$a = 5.222$, $c = 8.568$[a]	200.29	63.546	−1.3767	−0.1428
$ScZn_2$	$a = 5.2647$, $c = 8.4402$	$a = 5.2509$, $c = 8.4774$[b]	202.59	84.472	−2.5429	−0.3469

[a] From Ref. [28].
[b] From Ref. [18].

ing element A and B are put, respectively. N_A and N_B refer to the number of *A* and *B* atoms in unit cell, respectively. The calculated results of the cohesive energy are listed in Table 1. The negative cohesive energies of $MgZn_2$ and $ScZn_2$ show their energetic stabilization. From the calculated values, it can be further found that the cohesive energy of $ScZn_2$ is 1.1662 eV/atom lower than that of $MgZn_2$. Hence, $ScZn_2$ shows a higher structural stability than $MgZn_2$.

We also calculate the formation enthalpies ΔH [30], which can be calculated for binary alloy as

$$\Delta H = \frac{E_{tot} - N_A E^A_{\text{solid}} - N_B E^B_{\text{solid}}}{N_A + N_B} \quad (2)$$

where E^A_{solid} and E^B_{solid} are the energy per atom of pure elements with hexagonal structure for Mg, Sc and Zn in their ground state, and other quantities are the same as defined in Eq. (1). Negative formation enthalpy indicates an exothermic process, so $MgZn_2$ and $ScZn_2$ could be stable. Furthermore, the lower the formation enthalpy is, the stronger the stability is. It should be noted that the formation enthalpy of $ScZn_2$ is lower than that of $MgZn_2$, also indicating that the former is more stable than the latter.

3.2. Elastic properties

Elastic constants are the measure of the resistance of a crystal to an externally applied stress. For a material with hexagonal symmetry, there are six elastic constants (C_{11}, C_{12}, C_{13}, C_{33}, C_{44}, C_{66}), and only five of them are independent since $C_{66} = (C_{11} - C_{12})/2$ [31]. Elastic constants can be calculated by applying small strains to the equilibrium unit cell and determining the corresponding variations in the total energy. The elastic strain energy is given by

$$U = \frac{\Delta E}{V_0} = \frac{1}{2}\sum_{i}^{6}\sum_{j}^{6} C_{ij} e_i e_j \quad (3)$$

where $\Delta E = E_{\text{total}}(V_0,\varepsilon) - E_{\text{total}}(V_0,0)$, and it is the total energy difference between the deformed unit cell and initial unit cell. V_0 is the volume of equilibrium cell and C_{ij} is the elastic constant, which is the element of 6×6 elastic constant matrix in Voigt's notation. The necessary number of strains is determined by the crystal symmetry [31]. The strain tensor is given by

$$\varepsilon = \begin{pmatrix} e_1 & e_6/2 & e_5/2 \\ e_6/2 & e_2 & e_4/2 \\ e_5/2 & e_4/2 & e_3 \end{pmatrix} \quad (4)$$

For a hexagonal crystal, the five kinds of strains are listed in Table 2 [32]. For each kind of the above different strains of the lattice, the total energy has been calculated by imposing five appropriate deformations, ±2%, ±1% and zero, respectively. The calculated elastic constants are summarized in Table 3. Although there are no available experimental and theoretical data for elastic constants of $ScZn_2$ phase, the calculated elastic constants of Mg and $MgZn_2$ agree well with the other experimental values [33,34]. From calculated results in Table 3, it can be seen that for hcp Mg, $MgZn_2$ and $ScZn_2$ phases, C_{11} and C_{33} are very large among elastic constants, indicating that these phases are very incompressible under uniaxial stress along *x* (ε_{11}) or *z* (ε_{33}) axis.

Table 2
The strains used to calculate the elastic constants of $MgZn_2$ and $ScZn_2$.

Strain types	Strain tensor (unlisted: $e_i = 0$)	$\frac{1}{V_0}\frac{\partial^2 \Delta E}{\partial \delta^2}\Big\vert_{\delta=0}$
(δ, δ, 0, 0, 0, 0)	$e_1 = e_2 = \delta$	$C_{11} + C_{12}$
(0, 0, 0, 0, 0, δ)	$e_6 = \delta$	$1/4(C_{11} - C_{12})$
(0, 0, δ, 0, 0, 0)	$e_3 = \delta$	$1/2C_{33}$
(0, 0, 0, δ, δ, 0)	$e_4 = e_5 = \delta$	C_{44}
(δ, δ, δ, 0, 0, 0)	$e_1 = e_2 = e_3 = \delta$	$C_{11} + C_{12} + 2C_{13} + C_{33}/2$

From Ref. [32].

From Table 3, it is further found that the six elastic constants eventually become large from hcp Mg, $MgZn_2$ to $ScZn_2$. Because elastic constant measures the resistance to linear compression, when against compressing, $ScZn_2$ is the strongest, followed by $MgZn_2$, while hcp Mg is the weakest. The present results show the addition of Zn and Sc results in an increase of resistance to linear compression of the alloys.

The requirement of mechanical stability for hexagonal crystals leads to the following restrictions on the elastic constants [31]

$$C_{11} > 0, \quad C_{11} - C_{12} > 0, \quad C_{44} > 0, \quad (C_{11} + C_{12})C_{33} - 2C_{13}^2 > 0 \quad (5)$$

The calculated values of the elastic constants C_{ij} for $MgZn_2$ and $ScZn_2$ hexagonal crystals obey well all the above conditions, indicating the mechanical stability of $MgZn_2$ and $ScZn_2$ phases.

From the single crystal elastic constants, the polycrystalline elastic modulus is also estimated by the Voigt–Reuss–Hill (VRH) approximation [35]. The Voigt and Reuss approximations represent the maximum and minimum limits of the polycrystalline elastic modulus, respectively. For the hexagonal system, the Voigt bounds of *B* and *G* are

$$B_V = \frac{2}{9}\left(C_{11} + C_{12} + \frac{C_{33}}{2} + 2C_{13}\right) \quad (6)$$

$$G_V = \frac{1}{30}(7C_{11} - 5C_{12} + 12C_{44} + 2C_{33} - 4C_{13}) \quad (7)$$

And the Reuss bounds are

$$B_R = \frac{(C_{11} + C_{12})C_{33} - 2C_{13}^2}{C_{11} + C_{12} + 2C_{33} - 4C_{13}} \quad (8)$$

$$G_R = \frac{5}{2}\left\{\frac{[(C_{11} + C_{12})C_{33} - 2C_{13}^2]C_{44}C_{66}}{3B_V C_{44}C_{66} + [(C_{11} + C_{12})C_{33} - 2C_{13}^2](C_{44} + C_{66})}\right\} \quad (9)$$

Finally, the VRH mean values are obtained by

$$B = \frac{1}{2}(B_V + B_R) \quad (10)$$

$$G = \frac{1}{2}(G_V + G_R) \quad (11)$$

Table 3
The elastic constants C_{ij} (in GPa) of Mg, $MgZn_2$ and $ScZn_2$.

Material		Elastic constants					
		C_{11}	C_{12}	C_{13}	C_{33}	C_{44}	C_{66}
Mg	This work	63.10	23.14	20.45	69.70	18.99	19.98
	Exp.[a]	63.48	25.94	21.70	66.45	18.42	18.75
$MgZn_2$	This work	119.48	42.98	30.04	129.48	24.23	38.25
	Exp.[b]	107.25	45.45	27.43	126.40	27.70	30.90
$ScZn_2$	This work	155.73	52.14	47.73	154.92	47.88	51.78

[a] From Ref. [33].
[b] From Ref. [34].

Table 4
The elastic modulus (in GPa) and Poisson's ratio for Mg, $MgZn_2$ and $ScZn_2$ using Voigt, Reuss and Hill's approximations.

Material	B_V	B_R	B_H	G_V	G_R	G_H	E	E_a	E_c	G/B	ν
Mg	36.00	35.97	35.98	20.38	20.23	20.31	51.27	52.00	60.00	0.56	0.26
$MgZn_2$	63.84	63.83	63.84	35.03	32.31	33.67	85.91	101.00	119.00	0.53	0.28
$ScZn_2$	84.62	84.60	84.61	50.76	50.63	50.70	126.77	132.00	48.00	0.60	0.25

where the subscripts V and R designate the Voigt and the Reuss bounds. Further, the Young's modulus and Poisson's ratio can be obtained by using the bulk modulus and shear modulus

$$E = \frac{9BG}{3B+G} \tag{12}$$

$$\nu = \frac{3B-2G}{2(3B+G)} \tag{13}$$

The calculated results are shown in Table 4. It should be noted that the calculated bulk moduli of $MgZn_2$ and $ScZn_2$ are in accordance with those obtained through the fit to a Birch–Murnaghan EOS. The bulk modulus is usually assumed to be a measure of resistance to volume change by applied pressure [36], so the larger bulk moduli of $MgZn_2$ and $ScZn_2$ show that they have stronger resistance to volume change by applied pressure. Besides, shear modulus is a measure of resistance to reversible deformations upon shear stress [36]. The larger is the value of shear modulus, the more pronounced directional bonding is between atoms. The present calculated results demonstrate that $ScZn_2$ has the largest shear modulus, and then followed by $MgZn_2$ and Mg. Hence, the directional bonding in $ScZn_2$ would be much stronger than that in $MgZn_2$. Furthermore, Young's modulus provides a measure of stiffness of the solid. The larger is the Young's modulus, the stiffer is the material. From the calculated values we find that Young's modulus of $ScZn_2$ is 40.86 GPa larger than that of $MgZn_2$, indicating that $ScZn_2$ is much stiffer than $MgZn_2$. As indicated above, the elastic moduli of the two phases are larger than that of the pure Mg. Hence, it is obvious that the mechanical properties are improved after alloying.

The ratio of the shear modulus to bulk modulus of crystalline phases introduced by Pugh [36] can predict the brittle and ductile behavior of materials. A high (low) G/B value is associated with brittleness (ductility). The critical value separating ductility from brittleness is about 0.57. In the present work, the values of $MgZn_2$ and $ScZn_2$ are 0.53 and 0.60, respectively, implying that $MgZn_2$ is essentially ductile and $ScZn_2$ is slightly brittle. On the other hand, the Poisson's ratio could reflect the stability of a crystal against shear. The calculated results in Table 4 demonstrate that $ScZn_2$ is more stable against shear owing to its smaller value of Poisson's ratio.

3.3. Elastic anisotropy

The elastic anisotropy of crystals has an important application in engineering science since it is highly correlated with the possibility of inducing microcracks in materials [37]. The shear anisotropic factor provides a measure of the degree of anisotropy in the bonding between atoms in different planes. For hcp crystal, the shear anisotropy factors between $\langle 0\,1\,\bar{1}\,1\rangle$ and $\langle 0\,1\,\bar{1}\,0\rangle$ directions for the $\{1\,0\,\bar{1}\,0\}$ shear plane (between $\langle 1\,0\,\bar{1}\,1\rangle$ and $\langle 0\,0\,0\,1\rangle$ directions for the $\{0\,1\,\bar{1}\,0\}$ plane, between $\langle 1\,1\,\bar{2}\,0\rangle$ and $\langle 0\,1\,\bar{1}\,0\rangle$ directions for the $\{0\,0\,0\,1\}$ plane, respectively) are given by [36]

$$A_{\{1\,0\,\bar{1}\,0\}} = \frac{4C_{44}}{C_{11}+C_{33}-2C_{13}} \tag{14}$$

$$A_{\{0\,1\,\bar{1}\,0\}} = \frac{4C_{55}}{C_{22}+C_{33}-2C_{23}} \tag{15}$$

$$A_{\{0\,0\,0\,1\}} = \frac{4C_{66}}{C_{11}+C_{22}-2C_{12}} \tag{16}$$

The A value of unity means that the crystal exhibits isotropic property while values other than unity represent varying degrees of anisotropy [36]. The calculated values of $A_{\{1\,0\,\bar{1}\,0\}}$, $A_{\{0\,1\,\bar{1}\,0\}}$ and $A_{\{0\,0\,0\,1\}}$ for $MgZn_2$ and $ScZn_2$ are given in Table 5. It is seen that on $\{1\,0\,\bar{1}\,0\}$ and $\{0\,1\,\bar{1}\,0\}$ planes, $MgZn_2$ exhibits higher elastic anisotropy than $ScZn_2$. Meanwhile, $MgZn_2$ and $ScZn_2$ have isotropy on $\{0\,0\,0\,1\}$ plane, showing that the isotropy in this plane of the two precipitates meet the general property for hexagonal system. Overall, $ScZn_2$ exhibits better isotropy than $MgZn_2$.

To further investigate the elastic anisotropy of $MgZn_2$ and $ScZn_2$ phases, one also considers the anisotropy in linear bulk modulus. For hcp crystal, the linear bulk modulus along the a- and c-axes can be defined as follows [38]

$$B_a = a\frac{dp}{da} = \frac{\Lambda}{2+\beta} \tag{17}$$

$$B_c = c\frac{dp}{dc} = \frac{B_a}{\beta} \tag{18}$$

where

$$\Lambda = 2(C_{11}+C_{12}) + 4C_{13}\beta + C_{33}\beta^2 \tag{19}$$

$$\frac{1}{\beta} = \frac{B_c}{B_a} = \frac{C_{33}-C_{13}}{C_{11}+C_{12}-2C_{13}} \tag{20}$$

where β is defined as the relative change of the c-axis as a function of the deformation of the a-axis. So $1/\beta$ indicates the anisotropy of linear compressibility along the c-axis with respect to the a-axis. A value of unity implies the isotropic compressibility. The calculated values of B_a and B_c in Table 5 show that the anisotropy of $MgZn_2$ and $ScZn_2$ is also small because the ratios of B_c/B_a for them are close to unity.

Another way of measuring the elastic anisotropy is the percentage of anisotropy in compression and shear [39], which are defined as $A_B = (B_V - B_R)/(B_V + B_R)$ and $A_G = (G_V - G_R)/(G_V + G_R)$, respectively. The value of zero means that the crystal is isotropic, while 100% represents the maximum anisotropy. Table 5 lists the percentage of anisotropy in compression and shear for $MgZn_2$ and $ScZn_2$. It can be seen that both of materials exhibit small anisotropy in shear and compression. Interestingly, A_B shows $MgZn_2$ has better isotropy in compression, while A_G indicates $ScZn_2$ is more isotopic in shear.

However, the percentage anisotropy in compression and shear is not sufficient to evaluate the elastic properties of a crystal completely because they mainly provide measure of the degrees of

Table 5
The shear anisotropic factors, the linear bulk modulus B_a and B_c (in GPa), and the percentage of anisotropy in the compression A_B and shear A_G (in %).

Material	$A_{\{1\,0\,\bar{1}\,0\}}$	$A_{\{0\,1\,\bar{1}\,0\}}$	$A_{\{0\,0\,0\,1\}}$	A_G (%)	A_B (%)	B_a	B_c	$1/\beta$
$MgZn_2$	0.513	0.513	1.0	4.044	0.005	193.388	187.835	0.971
$ScZn_2$	0.890	0.890	1.0	0.134	0.011	257.926	245.942	0.954

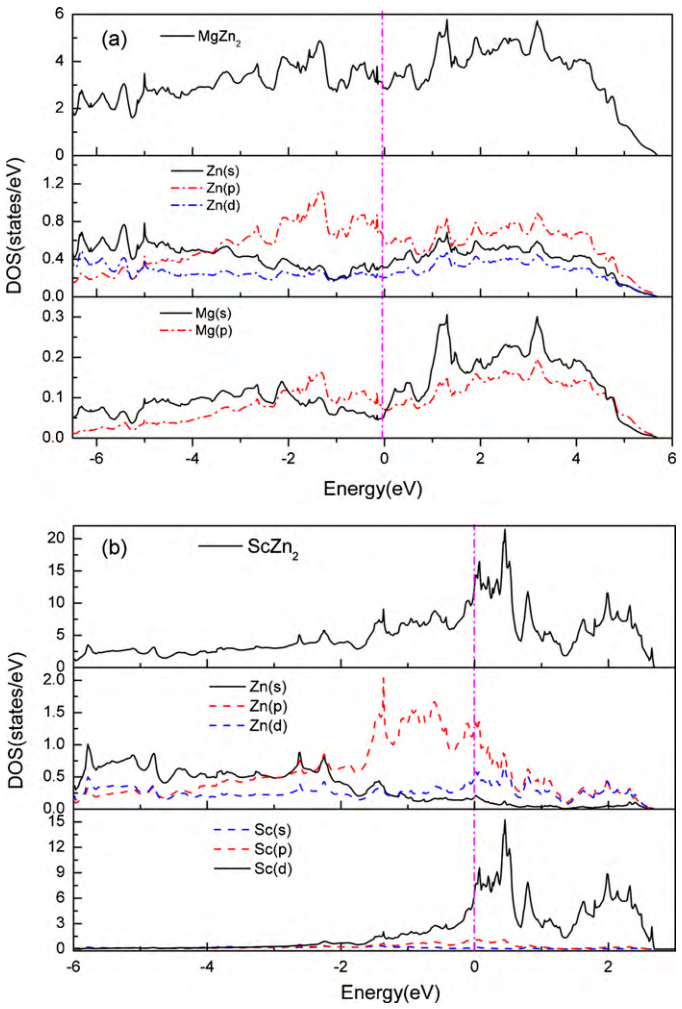

Fig. 2. The total and partial density of states (DOS) of $MgZn_2$ (a) and $ScZn_2$ (b), the Fermi level is set at zero energy and marked by the vertical lines.

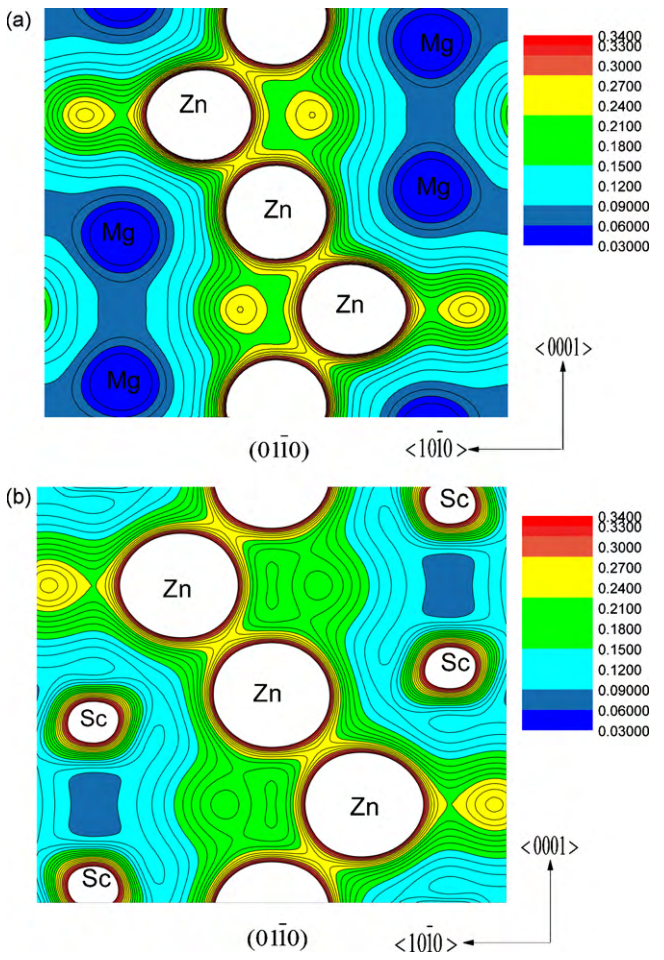

Fig. 3. The charge density distributions in eV/Å^3 on (0 1 $\bar{1}$ 0) plane for $MgZn_2$ (a) and $ScZn_2$ (b).

anisotropy in atomic bonding in different crystallographic planes [40]. For the hexagonal symmetry crystal, the in-plane anisotropy in *a*–*b* plane is nonexistent, only the in-plane elastic anisotropy in *a*–*c* plane is usually observed [41]. Another effective way of describing this in-plane elastic anisotropy is the directional dependence of Young's modulus, and it can be determined by the following equation [31]

$$\frac{1}{E} = (1 - l_3^2)^2 s_{11} + l_3^4 s_{33} + l_3^2(1 - l_3^2)(2s_{13} + s_{44}) \quad (21)$$

where S_{ij} are the elastic compliance constants and l_3 is the direction cosine. The calculated directional dependent Young's modulus E along *a*, *c* are given in Table 4. It also shows that both $MgZn_2$ and $ScZn_2$ exhibit small anisotropy. This in-plane elastic anisotropy can be understood by the nature of chemical bonding between atoms, which would be discussed in Section 3.4.

3.4. Electronic structures

In the present work, the electronic structure was calculated to get an insight into the bonding feature of $MgZn_2$ and $ScZn_2$, and further to reveal the underlying mechanism about structural stability and elastic properties of the two phases. The total DOS of $MgZn_2$ and $ScZn_2$ are presented in Fig. 2, along with the DOS of the constituent Mg, Sc and Zn. From the total and partial DOS of $MgZn_2$ shown in Fig. 2(a), it is found that the calculated total DOS exhibits metallic behavior, and it is mainly dominated by Mg 2s, 2p states and Zn 3d, 3p and 4s states. The hybridization between Mg and Zn is also clear in entire region and the variation of hybridization is small. Moreover, there is a so-called quasigap near the Fermi level which indicates the presence of the directional covalent bonding [42]. It is generally considered that the formation of covalent bonding would enhance the strength of material in comparison with the pure metallic bonding, so the quasigap near the Fermi level in the bonding region implies the system has a pronounced stability.

The DOS feature of $ScZn_2$ (see Fig. 2(b)) is different from $MgZn_2$ because the 3d electrons of Sc manifest a significant influence, and the 3p, 4s states in DOS of Zn distribute more broadly. Particularly, it is found that the density of states at Fermi level for $ScZn_2$ is higher than that of $MgZn_2$. The calculated bonding electron number of $ScZn_2$ per atom is 8.992 that is larger than 8.667 of $MgZn_2$. The higher is the number of bonding electrons, the stronger are the charge interactions [43]. Hence, $ScZn_2$ phase has higher structural stability than $MgZn_2$.

In order to further reveal the feature of bonding, the contour plots of charge density distributions are also investigated. Fig. 3(a) and (b) displays the calculated charge density distributions on (0 1 $\bar{1}$ 0) plane for $MgZn_2$ and $ScZn_2$, respectively. The contour lines are plotted from 0.03 to 0.34 eV/Å^3 with 0.015 eV/Å^3 interval. Higher density region corresponds to the core electron distribution of Mg, Zn and Sc atoms, and it contributes relatively little to the bonding. From Fig. 3(a), it can be seen clearly that there exists strong directional bonding between Zn and its nearest Zn atoms, while the bonding between Zn and Mg atom is mainly ionic. Fig. 3(b) also shows strong directional bonding between Zn atoms,

and ionic Sc–Zn bonding for $ScZn_2$. As shown in Fig. 3, it is obvious that the value of the charge density between Sc and Zn in $ScZn_2$ is larger than that between Mg and Zn in $MgZn_2$, so Sc–Zn bonding in $ScZn_2$ is slightly stronger than the Mg–Zn bonding in $MgZn_2$. In Fig. 3, the rather clear overlaps of electron densities between the neighbouring Zn atoms show the existence of covalent bonds, while the electron distribution around Mg(Sc) atoms exhibits a metallic bonding. The charge density distribution maps between Zn and Mg(Sc) atoms exhibit mainly ionic bonding with somewhat covalent feature. The present charge density distributions are consistent with the common feature of the electronic structure in AB_2 type Laves phases [44]. Generally, for AB_2 type Laves phase, there are mostly metallic bonding between *A* atoms, covalent bonding between *B* atoms and ionic bonding between *A* and *B* atoms.

4. Conclusions

In present paper, first-principles calculations have been performed to investigate the structural, elastic and electronic properties of $MgZn_2$ and $ScZn_2$ phases in Mg–Sc–Zn alloys. The calculated equilibrium lattice constants of both phases are in accordance with experimental values. The negative cohesive energy and formation enthalpy show structural stability of the two phases and the $ScZn_2$ phase is more stable from energetic point of view. The five independent elastic constants are calculated, showing that both phases are mechanically stable. The polycrystalline elastic parameters (B, G, E, A and ν) have been further calculated within the scheme of Voigt–Reuss–Hill (VRH) approximation. The ductility and plasticity, especially elastic anisotropies including the shear anisotropy factor, percentage of bulk and shear anisotropies and the linear bulk modulus are discussed in details. The electronic structure is analyzed for understanding of the underlying mechanism of the structural stability and mechanical properties of the two phases. According to the calculated electronic structure of both phases, the higher stability of $MgZn_2$ and $ScZn_2$ may be attributed to the directional covalent bonding. These results would be significant for the further optimization and design of Mg-rare earth alloys with excellent mechanical properties.

Acknowledgements

This work is supported by Natural Science Foundation of China (50861002), of Hunan Province (08JJ6001) and Guangxi Province (0991051), also Return Scholar Foundation of Chinese Minister of Education, Key Laboratory of Materials Design and Preparation Technology of Hunan Province (KF0803) and the Scientific Research Foundation of Guangxi University (X071117).

References

[1] S. Schumann, H. Friedrich, Mater. Sci. Forum 419–422 (2003) 51.
[2] B. Smola, I. Stulíková, F. Buch, B.L. Mordike, Mater. Sci. Eng. A 324 (2002) 113.
[3] L. Schlapbach, A. Züttel, Nature 414 (2001) 353.
[4] C. Potzies, K.U. Kainer, Adv. Eng. Mater. 6 (2004) 281.
[5] T.M. Pollock, Science 328 (2010) 986.
[6] G. Nayyeri, R. Mahmudi, F. Salehi, Mater. Sci. Eng. A (2010), doi:10.1016/j.msea.2010.05.040.
[7] Q. Xiang, R.Z. Wu, M.L. Zhang, J. Alloys Compd. 477 (2009) 832.
[8] K. Liu, J.H. Zhang, G.H. Su, D.X. Tang, L.L. Rokhlin, F.M. Elkin, J. Meng, J. Alloys Compd. 481 (2009) 811.
[9] C.M. Zhang, X. Hui, Z.G. Li, G.L. Chen, Mater. Lett. 62 (2008) 1129.
[10] X. Gao, J.F. Nie, Scripta Mater. 56 (2007) 645.
[11] L.Y. Wei, G.L. Dunlop, H. Westengen, Metall. Mater. Trans. A 26A (1995) 1947.
[12] J.B. Clark, L. Zabdyr, Z. Moser, in: A.A. Nayeb-Hashemi, J.B. Clark (Eds.), Phase Diagrams of Binary Magnesium Alloys, ASM International, Metals Park, OH, 1988, p. 353.
[13] X. Gao, J.F. Nie, Scripta Mater. 57 (2007) 655.
[14] X.Q. Zeng, Y. Zhang, L. Chen, W.J. Ding, Y.X. Wang, Y.P. Zhu, J. Alloys Compd. 395 (2005) 213.
[15] A. Kumar, A.K. Mukhopadhyay, K.S. Prasad, Mater. Sci. Eng. A 527 (2010) 854.
[16] Z.H. Huang, S.M. Liang, R.S. Chen, E.H. Han, J. Alloys Compd. 468 (2009) 170.
[17] Y. Kawamura, K. Hayashi, A. Inoue, T. Masumoto, Mater. Trans. 42 (2001) 1172.
[18] X.Y. Liu, F. Rau, J. Breu, K.J. Range, J. Alloys Compd. 243 (1996) L5–L7.
[19] P. Brommer, M. Boissieu, H. Euchner, S. Francoual, F. Gähler, M. Johnson, K. Parlinski, K. Schmalzl, Z. Kristallogr. 224 (2009) 97.
[20] A. Datta, U.V. Waghmare, U. Ramamurty, Acta Mater. 56 (2008) 2531.
[21] P. Hohenberg, W. Kohn, Phys. Rev. B 136 (1964) B864.
[22] G. Kresse, J. Furthmüller, Phys. Rev. B 54 (1996) 11169.
[23] C.S. Wang, B.M. Klein, H. Krakauer, Phys. Rev. Lett. 16 (1985) 1852.
[24] G. Kresse, D. Joubert, Phys. Rev. B 59 (1999) 1758.
[25] P.E. Blöchl, Phys. Rev. B 50 (1994) 17953.
[26] H.J. Monkhorst, J.D. Pack, Phys. Rev. B 13 (1976) 5188.
[27] P.E. Blöchl, O. Jepsen, O.K. Andersen, Phys. Rev. B 49 (1994) 16223.
[28] J. Yang, J.L. Wang, Y.M. Wu, L.M. Wang, H.J. Zhang, Mater. Sci. Eng. A 460 (2007) 296.
[29] F. Birch, J. Geophys. Res. 83 (1978) 1257.
[30] B.R. Sahu, Mater. Sci. Eng. B 49 (1997) 74.
[31] J.F. Nye, Physical Properties of Crystals, Clarendon Press, Oxford, 1964.
[32] X.H. Deng, B.B. Fan, W. Lu, Solid State Commun. 149 (2009) 441.
[33] L.J. Slutsky, C.W. Garland, Phys. Rev. 107 (1957) 972.
[34] T. Seidenkranz, E. Hegenbarth, Phys. Status Solidi (a) 33 (1976) 205.
[35] R. Hill, Proc. Phys. Soc. A 65 (1952) 349.
[36] S.F. Pugh, Phil. Mag. Ser. 7 (45) (1954) 823.
[37] V. Tvergaard, J.W. Hutchinson, J. Am. Ceram. Soc. 71 (1988) 157.
[38] P. Ravindran, L. Fast, P.A. Korzhavyi, B. Johansson, J. Wills, O. Eriksson, J. Appl. Phys. 84 (1998) 4891.
[39] D.H. Chung, W.R. Buessem, in: F.W. Vahldiek, S.A. Mersol (Eds.), Anisotropy in Single Crystal Refractory Compound, vol. 2, Plenum, New York, 1968, p. 217.
[40] K.B. Panda, K.S.R. Chandran, Comput. Mater. Sci. 35 (2006) 134.
[41] R. Yu, X.F. Zhang, L.L. He, H.Q. Ye, J. Mater. Res. 20 (2005) 1180.
[42] W. Lin, J.H. Xu, A.J. Freeman, Phys. Rev. B 45 (1992) 10863.
[43] C.L. Fu, X. Wang, Y.Y. Ye, K.M. Ho, Intermetallics 7 (1999) 179.
[44] W.Y. Yu, N. Wang, X.B. Xiao, B.Y. Tang, Solid State Sci. 11 (2009) 1400.